ACS APPLIED MATERIALS & INTERFACES

Research Article

www.acsami.org

Advance in Novel Boron Nitride Nanosheets to Nanoelectronic Device Applications

Muhammad Sajjad, Gerardo Morell, and Peter Feng*

Department of Physics, College of Natural Sciences, University of Puerto Rico, P.O. Box 70377, San Juan, Puerto Rico 00936-8377, United States

ABSTRACT: We report low-temperature synthesis of large-scale boron nitride nanosheets (BNNSs) and their applications for high-performance Schottky diode and gas sensor. Ten minutes of synthesis with a short-pulse-laser-produced plasma deposition technique yields a large amount of highly flat, transparent BNNSs. A basic reason for using short-pulse plasma beams is to avoid nanosheet thermal ablation or have low heat generated. Consequently, it greatly reduces the stress and yield large, flat BNNSs. The average size of obtained BNNS is around 10 μm and thickness is around 1.7 nm. Carbon element has been used for doping BNNSs and achieving BNNSs-based Schottky diode and gas sensing device. Typical current versus voltage characteristics of diode are examined. The breakdown reverse voltage is around −70 V. This probably indicates that the breakdown electric field of BNNSs-based diode is up to 1×10^8 V/cm. Sensing behavior of BNNSs-based gas sensor toward methane diluted with dry air is also characterized. The response time and recovery time are around 3 and 5 s at the operating temperature of 150 °C. Relatively, the sensor has poor sensitivity to oxygen gas.

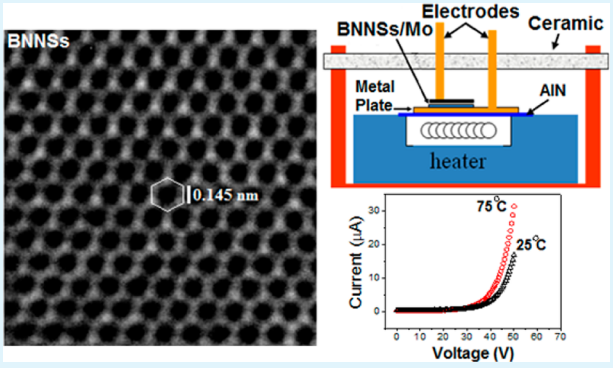

KEYWORDS: *synthesis, BNNSs, doping, Schottky diode, sensor*

INTRODUCTION

Discovery of graphene has brought a new revolution in the material science because of many charming, unusual properties and practical applications in nanoelectronic device technology.[1,2] This stimulates the interest in atomically thin sheets of other layered materials such as boron nitride nanosheets (BNNSs).[3] A single planar nanosheet of boron nitride (BN) is composed of few atomic layers in which alternating boron (B) and nitrogen (N) atoms construct a characteristic honeycomb network of B_3−N_3 hexagon with sp^2 bonding.[4,5] The B and N atoms are bound by covalent bonds, whereas weak van der Waals forces hold the layers together with an interplanar spacing of 0.334 nm. These nanosheets have similar lattice parameter and crystalline structure to that of graphene; therefore, they can possess enormous potential in comparable or complementary electronic and composite devices. For example, BNNSs have been considered ideal dielectric and substrate material to graphene-based nanoelectronic devices because it has an atomically smooth surface that is relatively free of dangling bonds and charge traps.[6] Moreover, excellent thermal, chemical stability and superb resistance to oxidation properties, soon lead this material to the new applications in high performance nanoelectronic devices.

BNNSs can be exfoliated or synthesized from bulk BN crystals by either mechanical cleavage or a chemical-solution-derived method.[7,8] However, with these synthesis methods, obtained nanosheets are of limited size which presents a problem in the application of this material for device technology. To solve this problem, several alternative synthetic routes, e.g., chemical vapor deposition (CVD)[9,10] and physical vapor deposition (PVD),[11] have been applied. These fabrication processes are complicated, time-consuming and yielding impure material.[12] For example, Yu et al.[13] conducted 180 min of CVD, but they were not able to find any BNNSs at the first 30 min of deposition. Moreover, high temperature (>700 °C) and ultrahigh vacuum (UHV) are required to synthesize BNNSs. Growth of BNNSs under UHV conditions appears to be self-limiting to one monolayer, and the growth of multilayers turns out to be difficult.[14]

Difficulty in synthesis of the high-band-gap electronic structure of BNNSs leads to some limitations for application in real electronic devices. To achieve desired electric and electronic properties for practical diode or transistor applications, doping of BNNSs layers is necessary to reconstruct the energy band gap in solids.[15−19] In general, BNNSs can be doped p-type with beryllium and n-type with boron, sulfur, and silicon or codoped with carbon and nitrogen. The best doping concentrations for BNNSs-based devices remain to be investigated. So far, it is reported that the combination of carbon (C) atoms with B and N atoms could possibly lead to the formation of different (B_x-C_y-N_z) layered structure.[20] Theoretical studies have also anticipated that the

Received: March 8, 2013
Accepted: May 11, 2013
Published: May 11, 2013

electronic structure and band gap of B_x-C_y-N_z would depend on composition and arrangement of B, C, and N elements in the lattice.[21] The dopant atoms incorporate in the crystalline structure and improve the electronic and semiconducting properties of the material.

In the present work, we produced defect free, atomically smooth, large scale BNNSs at significantly low substrate temperature (300 °C) using CO_2-pulsed laser deposition (CO_2–PLD) technique. For the first time, we have been able to use this material for the development of Schottky diode and gas sensor device at wafer scale. Current versus voltage (I–V) characteristics of the diode are thoroughly investigated at different temperatures, whereas gas sensing properties of the device are measured using oxygen (O) and methane (CH_4) as targeted gas.

EXPERIMENTAL CONDITIONS

The synthesis process is carried out by irradiating a commercial pyrolytic hexagonal boron nitride (h-BN) target (2 in. diameter, 0.125 in. thick, 99.99% purity, B/N ratio ≈ 1, density = 1.94 g/cm^3) using a CO_2–PLD technique (wavelength 10.6 μm, pulse width of 1–5 μs, repetition rate = 5 Hz, pulse energy 5 J, and power density 2×10^8 W/cm^2 per pulse). The advantage of short pulse deposition is to reduce the stress, whereas high power density of laser beam produces strong ablation of the target material, resulting in the formation of large scale BNNSs. The pressure in the deposition chamber was kept at 2.66×10^{-3} Pa. A molybdenum (Mo) disk used as a substrate was mounted onto substrate holder 3 cm away from the target. Prior to the deposition, Mo disk was polished with diamond nanopowder and cleaned with acetone and rinsed with deionized water to remove the surface impurities. The laser beam was focused with a 30 cm focal length ZnSe lens onto the target with an incident angle of 45° relative to the surface of rotating target (speed of ca. 200 rpm). The purpose of using a long focal length of the ZnSe lens is to control drift of plasma plume during deposition. The spot size of CO2 laser on the target is ~2×2 mm^2. Shift of the lens position in front of the target can be adjusted to control power density and size of plasma beam. A heater and a thermocouple were used to obtain and monitor the desired substrate temperature (300 °C). The duration for the deposition was kept 10 min.

CHARACTERIZATION METHODS

Transmission electron microscopy (TEM) was performed to characterize the nanostructure of as-grown BNNSs. We use a TEM equipped with an imaging aberration corrector, operated at 200 kV but with reduced illumination in order to avoid any possible knock on damage of ultrathin BNNSs. Raman scattering spectrum of BNNSs were also recorded at room temperature by using a triple monochomator (ISA J-Y Model T64000) with an excitation wavelength of 514 nm (Ar+ ion laser). Nanosheets were also surveyed using X-ray diffraction (XRD, Siemens- Bruker Diffractometer D5000).

Cycling test of sensing behavior of BNNSs-based gas sensor toward two different gases (O and CH_4) are conducted on the basis of calibration apparatus developed recently in our laboratory.[22] BNNSs sample is serially connected to a precise resistor and a battery to form a voltage–current–resistor (V–I–R) electrical circuit as a prototype sensor with simple contact of metal/BNNSs/metal architectures. Sensitive characters of the prototype were examined based on the measurement of the voltage drop across the precise resistor and the variation of the electrical conductivity of the sensor at different environments such as types of the gases (O and CH_4). The chamber for testing sensor properties is quite small (around 1000 mL) so that the change of gas concentration was instantaneous, which is a prerequisite condition for the accurate measurements of response and recovery time of the sensors. The detailed description of the system can be found out in our previous publication.[22]

To analyze the electronic properties of BNNSs, prototype of BNNSs-based Schottky barrier diode is fabricated. The current versus voltage (I–V) characteristics of diode are examined experimentally at different temperatures (25, 50, and 75 °C). Carbon doping in BNNSs produced Schottky barrier whose forward and reverse electrical characteristics are in excellent agreement with the characteristics of a simple PN junction diode.

RESULTS AND DISCUSSION

Microscopic images recorded from the surface of BNNSs are shown in figure 1. Low magnification TEM image of the sample

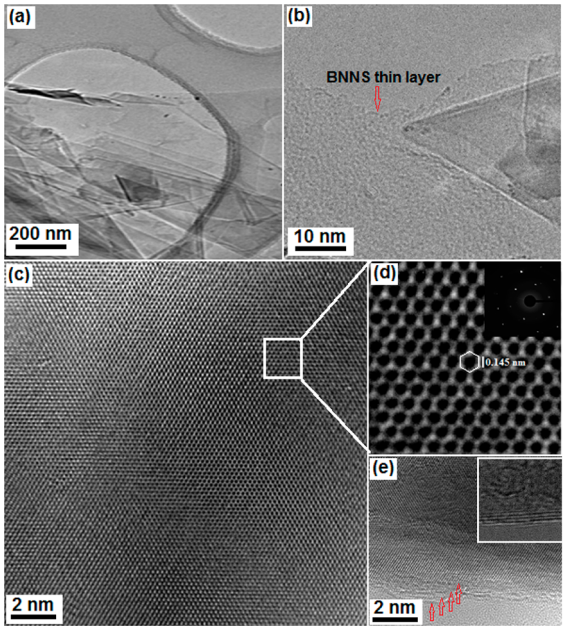

Figure 1. Electron micrographs of BNNSs: (a, b) low-magnification TEM images of several overlapped BNNSs, (b) TEM image of thin layer of BNNS, (c) HRTEM image when microscope was focused at the flat surface of the nanosheets, (d) magnified image of the selected area in c; the bright and slightly dull spots displays honeycomb structure of a six-membered B_3–N_3 hexagon. The inset shows ED pattern; indicating single crystalline structure. (e) Edge of BNNS shows four layers as marked with the arrows. The inset shows the magnified image of the edge of few-layer BNNSs. The scale bars are displayed on images.

shows large number of nanosheets mainly composed of several overlapped sheet structures (Figure 1a). Each nanosheet appears flat, sharped edge and transparent to the electron beam. The average size of obtained BNNS is around 10 μm. Figure 1b shows a thin BNNSs probably less than 1 nm in thickness. In order to analyze crystalline structure of BNNSs precisely, a single ultrathin boron nitride sheet is collected from the sample for further structural characterizations. This time, we used a high-resolution TEM (HRTEM) microscope equipped with an imaging aberration corrector, operated at 200 kV to directly characterize the crystalline structures of the single sheet as shown in Figure 1c. Densely packed honeycomb crystal lattice structure of six-membered B_3–N_3 hexagon probably belongs to a single or few atomic layer BNNSs is observed. In further magnifying image (Figure 1d), B_3–N_3 rings or two-dimensional benzene-like structures can be identified clearly. The shortest distance between the N and B atoms is around 0.145 nm along the (100) lattice direction that is consistent with the reported value for h-BN layer.[23] Within

dx.doi.org/10.1021/am400871s | ACS Appl. Mater. Interfaces 2013, 5, 5051–5056

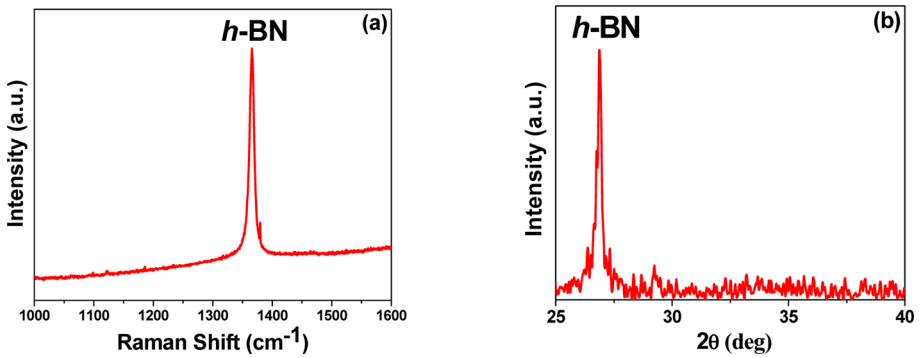

Figure 2. (a) Raman spectrum and (b) XRD pattern of BNNS material.

each layer of *h*-BN, B and N atoms are bound strongly by covalent bonds, whereas the atomic layers are held together by weak van der Waals forces.[24]

No defects from the BNNSs are detected (Figure 3c), though we operated the microscope at 200 keV, from which we could conclude that short pulse laser technique can be used to synthesize high quality, flat BNNSs. It should be mentioned here that previously reported data shows that the high-energy (≥80 keV) electron beam operated in TEM would damage atomic-layer of BNNSs.[25] The knock-on damage threshold for B atoms and N atoms in BN nanotubes are reported only 74 and 84 keV, respectively.[26] However, in the present work, the sheet was imaged for a very short time with reduced illumination that efficiently avoids any possibility of the knock-on damage of boron and nitrogen atoms within BN sheets. To date there is no report on the solution of the damage problem during atomic-thin film characterization with HRTEM with electron beam energy above 150 keV. Figure 1d shows the enlarged image of the selected area in Figure 1c. Neither N−N nor B−B bonds were observed in the characterized area; probable reason is that the B−N bonds are energetically preferable. The inset shows the ED pattern of the selected area of BNNSs. A series of diffraction spots arranged in typical hexagonal pattern probably indicates a single crystalline structure of synthesized BNNSs. This is in good agreement with the data obtained from HRTEM and Raman spectral measurements. The thickness of BNNSs is an important parameter that can be estimated by measuring the edge of BNNSs using TEM as shown in Figure 1e. The image shows a single BNNS consists of four to five stacked layers with 1.4 nm in thickness. The magnified image (inset in Figure 1e) shows clear pattern of the layer structure.

General interpretation of mechanism for the formation of BNNSs is as following. When the laser beam impacts the target surface, it generates a plasma plume out of the target surface directed toward the surface of substrates. This plasma plume is composed of high energy boron nitride ions and clusters. When these ions and clusters land onto the substrate, the extra thermal activation besides substrate heating provides energy exchange through collisions between active ions, clusters, and atoms of BN.[27,28] This helps to grow small BN layers that coalesce and transform into uniform BN nanosheets. Because of high thermal mobility, further incoming B and N ions and clusters land onto the surface of growing nanosheet would rapidly move along the sheet surface, reach the edge of the nanosheet, and covalently bond with the edge atoms before being re-evaporated. It is thus appears that during the first few minutes of deposition, BN layer grows parallel to the substrate surface. After the development of sufficient force onto the grain boundaries, the leading edge of the layer partially curled upward, which is an intrinsic property of 2D crystalline structure[29] or due to weak van der Wall force that connects deposited layer to the substrate surface.[30] Now, it could be possible that incoming BN species diffuse toward the surface of initially growing layer instead of toward the growing edges. In this process, a second layer starts growing on top of the first layer and so on. This process continues layer-by-layer, consequently a finite BN nanosheet obtained. Normally, nanosheets grow along the direction where the epitaxial energy of BN species is minimized. The detail mechanism of the nanosheets formation can be found in our recent publication.[31] BN species diffusing toward the substrate instead of toward the growing edges can be re-evaporated because of weak van der Waals forces attaching the species to the substrates. This mechanism accounts for the observation that rather than the formation of a single continuous BN layer parallel to the substrate, we observe self-assembly of multiple sets of BNNSs.

Figure 2a shows a typical Raman spectrum of BN nanosheets. An intense line centered at 1365 cm^{-1} indicating Raman active E_{2g} vibrational mode is related to hexagonal phase.[32,33] The extremely narrow Raman peak probably suggests that the obtained BNNSs have less defect concentrations. Compared with the results from a traditional CVD method that in most cases yields high level of impurities inside the samples, the present plasma pulse beam deposition technique could produce high purity of BNNSs. Figure 2(b) shows XRD pattern of nanosheets where a single 2θ peak is detected at ∼26.84° that further confirmed *h*-BN (002) phase[34,35] in BNNSs. No other characteristic peak associated with impurity elements was detected in Raman and XRD spectra.

After characterization of crystalline structure of the samples, a prototype of BNNSs-based gas sensor is designed and fabricated. A good sensor has several important parameters for example, sensitivity, selectivity, response time and recovery time, as well as repeatability. To investigate these properties in our sensor, the static and dynamic testing of the sensor device for different gases at the same concentration was performed. A chamber was employed to provide different gas concentration levels in incremental steps, while temperature remained unchanged at 150 °C. Each step was maintained at constant parameters till the voltage reading reached a steady value. The sensing mechanism is based on the resistance change caused by the reaction of the absorbed gas molecules at the surface of BNNSs. Basically, sensor comprises of chip (micrometer) scale metal fringes (electrodes), sensing element (BNNSs), a heater,

dx.doi.org/10.1021/am400871s | ACS Appl. Mater. Interfaces 2013, 5, 5051−5056

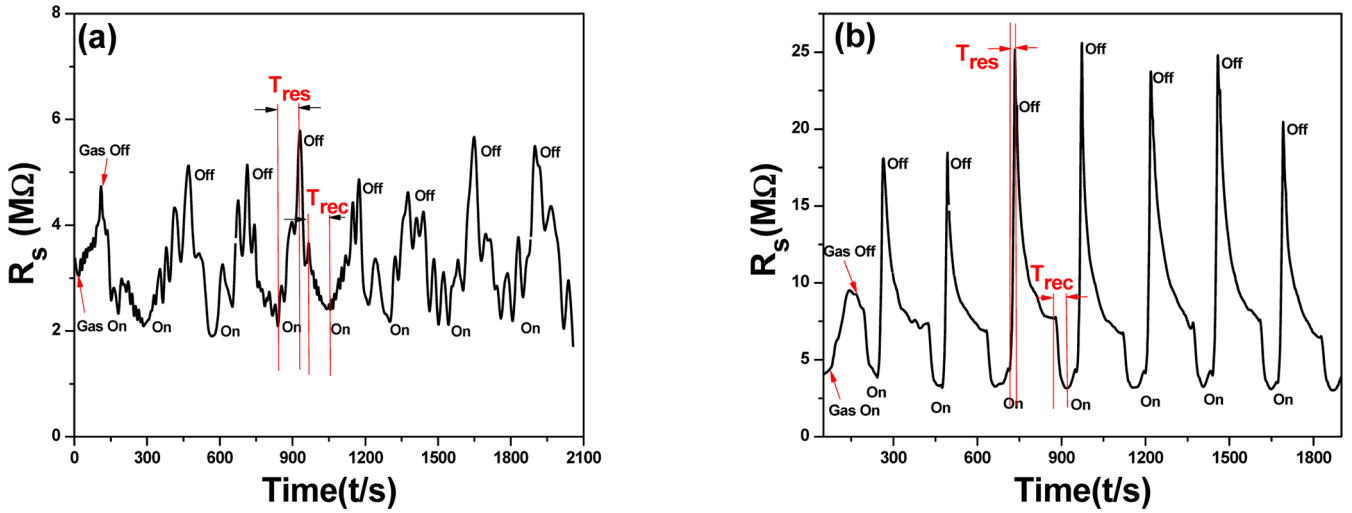

Figure 3. Variation in the resistance of sensor to (a) O and (b) CH_4 gas.

power supply, and electric digit meter. Cycling tests of sensing behaviors of newly designed sensors are conducted in a calibrated apparatus.[22] Oxygen (O) and methane (CH_4) gases are used independently as the targeted gases for eight cycles, from which the response time (T_{res}) and recovery time (T_{rec}) of the sensor are investigated as shown in panels a and b in Figure 3.

The sensitivity (S) of the sensor is defined as $S(\%) = (R_s - R_v)/R_v$, where R_s represents the resistance of the sensor when gas is introduced in the chamber and R_v is the resistance in vacuum.[36] When sensor is exposed with the gas (O or CH_4), the corresponding change in resistance is recorded as shown in panels a and b in Figure 3. The value for "S" is calculated from the cycle in which maximum change in the resistance is recorded. In the case of O gas at (100 ppm), the maximum value of "S" was recorded around 1.5 when the output signal was stable, whereas T_{res} and T_{rec} were around 70−80 s and 100−110 s, respectively as shown in Figure 3a. In contrast, for the case of CH_4 gas (Figure 3b), at the same gas concentration, the change in resistance of the sensor upon exposure of gas is much stronger. The relative intensity of the signal recorded for CH_4 is much larger than that for O gas, indicating BNNSs-based sensor has high sensitivity ($S \approx 7.8$) or selective properties. The possible reason is that methane molecules are polarized, thus they can easily be absorbed by the surface and grain boundaries of BNNSs and then change the conductivity of BNNSs. Furthermore, T_{res} (≈ 10−15 s) and T_{rec} (≈ 15−20 s) are recorded down to few seconds. Actual T_{res} and T_{rec} should be even shorter than the observed value. This is because in the present case, time delay in switching on or off the valves of gas inlet and outlet as well as low pumping capacity (7 m^3/h) affect the measurement results.

Eight cycles of experimental testing showed that the sensor has good repeatability. But it is noticed that in the first cycle when gas is introduced into the chamber, the response of the sensor is not unique. A tentative interpretation is that the contamination (humidity or dust particles) on the surface of BNNSs affects the sensitivity of the sensor. After first cycle, response and repeatability of the sensor in each cycle of gas "in" and "out" is almost identical. This is due to the fact that the impurities from the surface of BNNSs might be pumped out with the gas. When the gas is switched off, the resistance of the sensor drops slowly. There are two possible steps involved after switch off the gas. In the first step, gas molecules are pumped out from the chamber. During this interval of time (between the T_{res} and the T_{rec}), large amount of gas is still adsorbed on the surface of BNNSs. Consequently, the conductivity or response of sensing material changes slowly as evidenced shown in each cycle. In the second step, continuous pumping results in quick desorption of gas molecules from the surface of BNNSs. Slight variation in the numbers of molecules on the surface of BNNSs can cause large change of electrical properties of BNNSs. That is why during this step, signal drops rapidly.

BNNSs-based gas-sensors operate by measuring changes in electrical resistance of the BNNSs upon exposure to the gas. Though the exact mechanism still remains to be investigated, it appears that free electrons can move easily through the surface and across the boundaries of BNNSs. General understanding/explanation is that when gas is introduced in the chamber, it is adsorbed onto the surfaces as well as at the boundaries of BNNSs that removes free electrons, creating a potential barrier. This is manifested as an increase in resistance of the sensor.

Besides gas sensor, much attention has also been paid in the fabrication of BNNSs-based Schottky diode. Two types of junction: pure BNNSs/metal and doped-BNNSs/metal, have been fabricated and tested. The doping process is completed by exposing nanosheets via cold plasma.[37] A low-pressure (10 Pa) CH_4 was used with dc plasma ignited between two electrodes. The BNNSs were kept 5 cm away from the discharge zone. The doped BNNSs were placed back to the device in order to analyze I−V characteristics of Schottky diode. The fabricated device to record the $I-V$ characteristics of diode is shown in block diagram (Figure 4). As, the entire surface of substrate was covered with randomly oriented BNNSs, we setup electrodes on the surface of BNNSs/Mo substrate by electronic soldering method. For the precise $I-V$ measurements, setup is connected with a Keithley 6517A electrometer in order to characterize electronic properties of BNNSs.

$I-V$ characteristics for the case of pure BNNSs/metal junction are recorded at different temperatures (25 °C, 50 °C, and 75 °C) as shown in Figure 5a. Generally, high temperature would cause a decrease in the resistance of BNNSs, resulting in an increase of electric current at the certain voltage. At a fixed temperature, current increased almost linearly with the applied voltage (Figure 5a). This indicates that the active region between the pure BNNSs and metal substrate has no Schottky

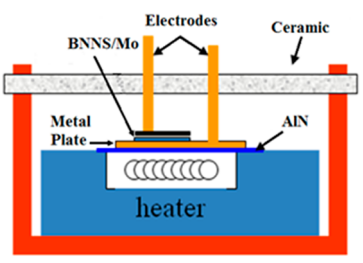

Figure 4. Block diagram of the device prepared to analyze the characteristics of BNNSs-based Schottky diode.

contact, whereas the junction based on doped BNNSs shows diodic behavior indicating the formation of Schottky contact between the BNNSs and metal substrate ((Figure 5b, c). Figure 5b shows $I-V$ characteristics of Schottky diode recorded at 25 and 75 °C, respectively. It seems that variation of temperature has an obviously affect in forward current of diode. At sufficiently high temperatures, a substantial amount of current can be observed.

The complete curves shown in Figure 5c appear has a typical behavior of a simple PN junction diode: its tendency to conduct electric current in only one direction. Normally, the curve can be divided into four areas. At very large reverse bias, beyond the peak inverse voltage (−73 V), a process called reverse breakdown occurs that causes a large increase in current that usually damages the diode permanently. Here it should be mentioned that because the thickness of membrane of the BNNSs is less than 10 nm, experimental data indicate that the breakdown of electric field value is up to 7.3×10^7 V/cm. These characteristics are directly attributing the outstanding properties of BNNSs as a material for electronic applications. The second region, at reverse biases has only a very small reverse saturation current. In the reverse bias region for a normal P−N junction diode, the current through the device is very low (in few μA ranges). The third region is forward with forward bias voltage less than 45 V, where only a small forward current is conducted. As the potential difference is increased up to or above V_d = 45 V (forward voltage drop), the diode current becomes appreciable, and the diode presents a very low resistance. The current−voltage curve is exponential.

CONCLUSIONS

In summary, experimental data proved that the BNNSs are an ideal material for electrical and gas sensing applications. Pulsed CO_2 laser plasma deposition technique provides a feasible method for the growth of flat and transparent BNNSs on large area at significantly low substrate temperature. HRTEM study revealed that BNNSs consists of a large amount of highly ordered boron and nitrogen atoms packed in 2D benzene-like structures. Such atomic structures of BNNSs are highly sensitive to CH_4 while comparatively less sensitive to oxygen. High-band-gap semiconductor BNNSs can be used to fabricate typical Schottky diodes and transistors. Carbon doping in BNNSs produce Schottky barrier diode whose forward and reverse electrical characteristics are in excellent agreement with the characteristics of a simple PN junction diode. Such diodes operate at higher temperature and give rise to the forward current at about 35 μA, whereas the leakage current remains small until reverse voltage reaches to the breakdown point (−73 V). The high breakdown electric field almost up to 1×10^8 V/cm indicating excellent stability of the device in forward and reverse biased conditions that can lead this material to various electronic applications where high voltage is desired.

AUTHOR INFORMATION

Corresponding Author

*E-mail: peter.feng@upr.edu.

Notes

The authors declare no competing financial interest.

ACKNOWLEDGMENTS

This work is supported by the NASA-EPSCoR seed grants (NASA Cooperative Agreement NNX13AB22A and NNX07AO30A) and DoD grant. We would like to thank Dr. Maxime Guinel and his staff for TEM measurements at the Nanoscopy Facility sponsored by NSF (NSF Cooperative Agreement 1002410). We also acknowledge fellowship support from UPR-DEGI.

REFERENCES

(1) Novoselov, K. S.; Geim, A. K.; Morozov, S. V.; Jiang, D.; Katsnelson, M. I.; Grigorieva, I. V.; Dubonos, S. V.; Firsov, A. A. *Nature* **2005**, *438*, 197.

(2) Novoselov, K. S.; Geim, A. K.; Morozov, S. V.; Jiang, D.; Zhang, Y.; Dubonos, S. V.; Grigorieva, I. V.; Firsov, A. A. *Science* **2004**, *306*, 666.

(3) Zeng, H.; Zhi, C.; Zhang, Z.; Wei, X.; Wang, X.; Guo, W.; Bando, Y.; Golberg, D. *Nano Lett.* **2010**, *10*, 5049.

(4) Meyer, J. C.; Chuvilin, A.; Algara, S. G.; Biskupek, J.; Kaiser, U. *Nano Lett.* **2009**, *9*, 2683.

(5) Alem, N.; Erni, R.; Kisielowski, C.; Rossell, M. D.; Gannett, W.; Zettl, A. *Phy. Rev. B* **2009**, *80*, 155425.

(6) Lee, K. H.; Shin, H. J.; Lee, J.; Lee, I.; Kim, G.; Choi, J. Y.; Kim, S. W. *Nano Lett.* **2012**, *12*, 714.

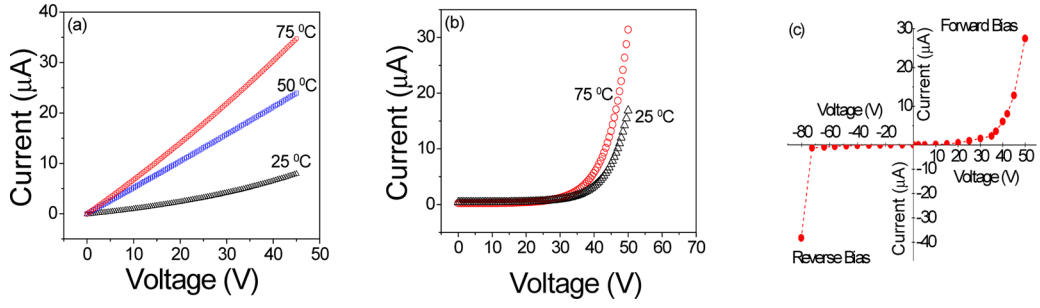

Figure 5. Effect of temperature on $I-V$ characteristics of Schottky diode, (a) undoped BNNSs, (b) doped BNNSs, and (c) forward and reverse biased characteristics of doped BNNSs at room temperature.

(7) Lin, Y.; William, T. V.; Connel, J. W. *J. Phys. Chem. Lett.* **2010**, *1*, 277.
(8) Zhi, C.; Bando, Y.; Tang, C.; Kuwahara, H.; Golberg, D. *Adv. Mater.* **2009**, *21*, 2889.
(9) Kim, K. K.; Hsu, A.; Jia, X.; Kim, S. M.; Shi, Y.; Hofmann, M.; Nezich, D.; Rodriguez-Nieva, J. F.; Dresselhaus, M.; Palacios, T.; Kong, J. *Nano Lett.* **2012**, *12*, 161.
(10) Song, L.; Ci, L.; Lu, H.; Sorokin, P. B.; Jin, C.; Ni, J.; Kvashnin, A. G.; Kvashnin, D. G.; Lou, J.; Yakobson, B. I.; Ajayan, P. M. *Nano Lett.* **2010**, *10*, 3209.
(11) Anzai, A.; Nishiyama, F.; Yamanaka, S.; Inumaru, K. *Mater. Res. Bull.* **2011**, *46*, 2230.
(12) Gardiner, R.; Buskirk, P.; Kirlin, P. U. S. Patent 5 362 328.
(13) Yu, J.; Qin, L.; Hao, Y.; Kuang, S.; Bai, X.; Chong, Y. M.; Zhang, W.; Wang, E. *ACS Nano* **2010**, *4*, 414.
(14) Nagashima, A.; Tejima, N.; Gamou, Y.; Kawai, T.; Oshima, C. *Phys. Rev. B* **1995**, *51*, 4606.
(15) Giovannetti, G.; Khomyakov, P. A.; Brocks, G.; Paul, J. K.; Jeroen, van, D. B. *Phys. Rev. B* **2007**, *76*, 073103.
(16) Du, A.; Smith, S. C.; Lu, G. *Chem. Phys. Lett.* **2007**, *447*, 181.
(17) Zhang, Z.; Guo, W. *Phys. Rev. B* **2008**, *77*, 075403.
(18) Ci, L.; Song, L.; Jin, C.; Jariwala, D.; Wu, D.; Li, Y.; Srivastava, A.; Wang, Z. F.; Storr, K.; Balicas, L.; Liu, F.; Ajayan, P. M. *Nat. Mater.* **2010**, 1−6.
(19) Zhang, H. X.; Feng, P. X. *ACS: Appl. Mater. Interfaces* **2012**, *4*, 30.
(20) Rubio, A. *Nat. Mater.* **2010**, *9*, 379.
(21) Rubio, A.; Corkill, J. L.; Cohen, M. *Phys. Rev. B* **1994**, *49*, 5081.
(22) Feng, P. X.; Zhang, H. X.; Peng, X. Y.; Sajjad, M.; Chu, J. *Rev. Sci. Instrum.* **2011**, *82*, 043303.
(23) Zhi, Y. C.; Bando, Y.; Tang, C. C.; Kuwahara, H.; Golberg, D. *Adv. Mater.* **2009**, *21*, 2889.
(24) Pakdel, A.; Zhi, C.; Bando, Y.; Nakayama, T.; Golberg, D. *ACS Nano* **2011**, *5*, 6507.
(25) Meyer, J. C.; Chuvilin, A.; Siller, G. A.; Biskupek, J.; Kaiser, U. *Nano Lett.* **2009**, *9*, 2683.
(26) Zobelli, A.; Gloter, A.; Ewels, C. P.; Seifert, G.; Colliex, C. *Phys. Rev. B* **2007**, *75*, 245402.
(27) Mirkarimi, P. B.; Medlin, D. L.; McCarty, K. F.; Barbour, J. C. *Appl. Phys. Lett.* **1995**, *66*, 2813.
(28) Sajjad, M.; Zhang, H. X.; Peng, X. Y.; Feng, P. X. *Phys. Scr.* **2011**, *83*, 065601.
(29) Nemanich, R. J.; Solin, S. A.; Martin, R. M. *Phys. Rev. B* **1981**, *23*, 6348.
(30) Yu, J.; Qin, L.; Hao, Y.; Kuang, S.; Bai, D. X.; Chong, M. Y.; Zhang, W.; Wang, G. E. *ACS Nano* **2010**, *4*, 414.
(31) Sajjad, M.; Ahmadi, M.; Guinel, M. J-F.; Lin, Y.; Feng, P. X. *J. Mater. Sci.* **2012**, 1−5.
(32) Nag, A.; Raidongia, K.; Hembram, K. P. S. S.; Datta, R.; Waghmare, U. V.; Rao, C. N. R. *ACS Nano* **2010**, *4*, 1539.
(33) Hoffman, M. M.; Doll, G. L.; Eklund, P. C. *Phys. Rev. B* **1984**, *30*, 6051.
(34) Zhang, W. J.; Matsumoto, S. *Chem. Phys. Lett.* **2000**, *330*, 243.
(35) Zhang, W. J.; Matsumoto, S. J. *Mater. Res.* **2000**, *15*, 2677.
(36) Peng, X. Y.; Sajjad, M.; Chu, J.; Yang, B. Q.; Feng, P. X. *Appl. Surf. Sci.* **2011**, *257*, 4795.
(37) Zhang, H. X.; Feng, P. X. *ACS Appl. Mater. Interfaces* **2012**, *4*, 30.